Carbohydrate Polymers 157 (2017) 1611–1619

Contents lists available at ScienceDirect

Carbohydrate Polymers

journal homepage: www.elsevier.com/locate/carbpol

Size effect of ZnO nanorods on physicochemical properties of plasticized starch composites

L. Guz[a], L. Famá[a], R. Candal[b,*], S. Goyanes[a,*]

[a] Universidad de Buenos Aires. Facultad de Ciencias Exactas y Naturales, Departamento de Física, Laboratorio de Polímeros y Materiales Compuestos (LPM&C). Instituto de Física de Buenos Aires (IFIBA-CONICET). Ciudad Universitaria (1428), Ciudad Autónoma de Buenos Aires, Argentina
[b] Instituto de Investigación e Ingeniería Ambiental, CONICET, Universidad Nacional de San Martín, 25 de Mayo y Francia (1650), San Martín, Provincia de Buenos Aires, Argentina

ARTICLE INFO

Article history:
Received 27 August 2016
Received in revised form 9 November 2016
Accepted 12 November 2016
Available online 15 November 2016

Keywords:
Starch composite
ZnO nanorods size
Biodegradability
Bactericidal activity

ABSTRACT

This work demonstrates that the size of ZnO nanorods (ZnONR) with similar aspect ratio determines several physicochemical and microbiological properties of thermoplastic starch composites (TPS/ZnONR) at a given concentration of ZnONRs. A combination of sol-gel and hydrothermal methods was developed to synthesize ZnONR with different sizes but similar aspect ratios. Starch composites containing 1 wt.% of ZnONR were prepared by casting. Composites with smaller size nanorods (ZnONR-S) showed more efficiency in shielding UVA radiation and had a higher solubility and water vapor permeability than those with larger nanorods (ZnONR-L). Mechanical properties, biodegradability and antibacterial activity were also influenced by the size of the ZnONR. X-ray diffraction analysis showed that composites with ZnONR-S maintained the typical B-V type starch structure, intensifying the V-type starch structure peaks, while composite with ZnONR-L induced the formation of an amorphous structure, preventing starch retrogradation during storage. Properties affected by nanorods size are fundamental in determining composite applications.

1. Introduction

In recent years, the increasing concern regarding environmental disposal of petroleum-based plastics led to the development of new biodegradable materials. Several natural biopolymers and biodegradable plasticizers have been investigated as new materials for production of biodegradable plastics (Siracusa, Rocculi, Romani, & Rosa, 2008; Vieira, da Silva, dos Santos, & Beppu, 2011). One of the most studied biopolymers is starch, which is a low cost biopolymer from renewable resources (Jiménez, Fabra, Talens, & Chiralt, 2012) and gives origin to films (Famá, Bittante, Sobral, Goyanes, & Gerschenson, 2010). However, its hydrophilic nature leads to films with high water permeation and solubility (Bertuzzi, Castro Vidaurre, Armada, & Gottifredi, 2007; Laohakunjit & Noomhorm, 2004), as well as poor mechanical properties (Cano et al., 2015; Gutiérrez, Tapia, Pérez, & Famá, 2015). Several approaches have been studied in order to overcome starch films limitations. The incorporation of nanoparticles as fillers is one of the most explored alternatives in the literature with great results (Arora & Padua, 2010; de Azeredo, Mattoso, & McHugh, 2011; Xie, Pollet, Halley, & Avérous, 2013). Most of the investigations focus on the effect of the nanofiller concentration in the starch matrix films (Angles & Dufresne, 2001; Morales, Candal, Famá, Goyanes, & Rubiolo, 2015) or the aspect ratio of the filler, which is one of the most important parameters that affects matrix/nanoparticle interaction, mechanical and barrier properties of the composites (Chen, Liu, Chang, Anderson, & Huneault, 2009; Chen, Liu, Chang, Cao, & Anderson, 2009; Soykeabkaew, Supaphol, & Rujiravanit, 2004). However, the effect of nanofillers with similar aspect ratio and geometry but different size is poorly understood.

Zinc oxide nanoparticles are a very interesting additive used in different types of coatings and composites due to their great and innovative characteristics such as antibacterial and UV shielding capacity (Shankar, Teng, Li, & Rhim, 2015). Besides, ZnO is considered Generally Regarded as Safe (GRAS) by the FDA in plastics and food contact materials (FDA 21CFR178.3297). Recently, the European Food Safety Authority (EFSA) recommended its use in polymers in contact with food up to 2%wt. (EFSA Panel on Food Contact Materials, 2016), meaning that in certain dose it can be used as reinforcement in polymers for food packaging. Several authors have proposed the use of ZnO nanoparticles as fillers in poly-

* Corresponding authors.
E-mail addresses: rjcandal@gmail.com (R. Candal), goyanes@df.uba.ar, sgoyanes@gmail.com (S. Goyanes).

http://dx.doi.org/10.1016/j.carbpol.2016.11.041
0144-8617/

mer composites for active food packaging with the aim to inhibit pathogenic bacterial growth and food spoilage (Arfat, Benjakul, Prodpran, Sumpavapol, & Songtipya, 2014; Emamifar, Kadivar, Shahedi, & Soleimanian-Zad, 2010; Kanmani & Rhim, 2014; Pantani, Gorrasi, Vigliotta, Murariu, & Dubois, 2013; Shankar et al., 2015). Morsy et al. (2014) demonstrated the effectiveness of ZnO nanoparticles incorporation in pullulan, a polysaccharide obtained from the fungal organism *Aureobasidium pullulans*, nanocomposite films as active packaging for the preservation of raw beef and turkey breast (Morsy, Khalaf, Sharoba, El-Tanahi, & Cutter, 2014).

Between the different types of ZnO nanoparticles, nanorods presents several advantages since they have a high surface to volume area, good tensile behavior (Wang, Kulkarni, Ke, Bai, & Zhou, 2008) and great antibacterial capacity (Nair et al., 2009). These properties suggest that the incorporation of ZnO nanorods to starch films may lead to an active packaging material with antimicrobial activity, preserving food for longer time periods.

There are some reports about the influence of the concentration of ZnONR incorporated in starch films as nanofillers (Alebooyeh, Nafchi, & Jokr, 2012; Nafchi, Alias, Mahmud, & Robal, 2012; Nafchi, Nassiri, Sheibani, Ariffin, & Karim, 2013) but, to our knowledge, there are no reports on the effect of the size of ZnONR, with the same aspect ratio, in starch films nanocomposites properties.

The goal of this work is to explore the effect of the size of ZnONR with similar aspect ratio, isoelectric point, crystalline structure and polar to non-polar plane ratio on the physicochemical properties of thermoplastic starch (TPS)/ZnONR composites. In this sense, two TPS/ZnONR composites containing 1 wt.% ZnONR were prepared. Each composite contained monodispersed ZnONR with different size. The chosen wt.% guarantee the homogeneous distribution of ZnONR in the matrix and a notable effect on physicochemical properties (see for example (Nafchi et al., 2013), and Supplementary Fig. 1). Size effect of the ZnONR on the morphological, thermal and structural characteristics, as well as water vapor permeability, mechanical properties, biodegradability and antibacterial activity on starch composites was determined.

2. Materials and methods

2.1. ZnO nanorods synthesis and characterization

ZnO nanorods synthesis was based on the previous works of Chen, Qiao, Liu, and Yang (2009) and Yi, Choi, Jang, Kim, and Jung (2007). The strategy of the synthesis was a combination of sol-gel with hydrothermal growth, using tetramethylammonium hydroxide ($(CH_3)_4NOH$, A. R, Fluka) as a structure-directing agent. ZnO nanoparticles used as seeds were prepared by sol–gel method. 50 mL of a 0.030 M solution of NaOH in methanol were added drop wise to 50 mL of a 0.020 M solution of $Zn(CH_3COO)_2$ dissolved in methanol and reflux heated at 60 °C for 2 h. The nanoparticle suspension was then cooled to room temperature and 2.5 mL tetramethylammonium hydroxide was added into the suspension. The suspension was sonicated in an ultrasonic bath (tb02 Testalab) for 30 min and stored at 4 °C. ZnONR with different size but similar aspect ratio were obtained using growing solutions with different concentration of Zn(II) and hexamethylenetetramine (HMT) but the same concentration of seeds. 3.0 mL of ZnO seeds suspension was added to 90 mL of an aqueous solution 8.0 mM or 15 mM in both $Zn(NO_3)_2{\cdot}6H_2O$ and HMT and heated at 90 °C for 3 h. The precipitates were collected by ultracentrifugation, washed several times with deionized water and dried at 50 °C in a vacuum oven for 12 h. The different ZnONR powders were named ZnONR-S and ZnONR-L for concentrations of Zn(II) in the growing solutions of 8.0 mM and 15 mM respectively. The morphologies of the obtained ZnONR were determined by scanning electron microscopy (FEG-SEM Zeiss Supra 40). The size of the obtained nanorods was determined using ImageJ software image analyzer. 100 rods were measured to obtain width and length size distributions. The XRD patterns were recorded on a Siemens D5000 X-ray diffractometer (Cu Ka). Electrophoretic mobility of ZnONR in 1 mM KCl solution was determined with a Brookhaven 90 Plus/Bi-100 MAS.

2.2. Films preparation

Thermoplastic starch films (TPS) were prepared by casting according to Famá, Rojo, Bernal, and Goyanes (2012). An aqueous suspensions containing cassava starch (4.5 g/100 g of system), glycerol (1.5 g/100 g of system) and distillate water (94.0 g/100 g of system) was stirred at room temperature during 45 min at constant agitation of 250 rpm. After that, the mixture was heated up to 80 °C with a 3 °C/min ramp and kept at this temperature for 5 min under stirring at the same rpm. After the heating step, the suspensions were degassed with a vacuum pump for 5 min, cast in glass Petri dishes and dried at 50 °C during 48 h. In the case of the composites (TPS/ZnONR), ZnONR-S or ZnONR-L (1 wt.% of solids) were dispersed in the amount of distilled water and glycerol used in TPS preparation (previously to be mix with the starch), with ultrasonic bath for 30 min. Then, the same procedure for TPS was done to obtain the composites films. Preliminary results showed that higher concentrations of ZnONR (2 wt.% of solids) tend to agglomerate in the composite (see Supplementary Fig. 1); also, the legislation does not permit more than 2 wt.% (EFSA Panel on Food Contact Materials, 2016). All the films were stored for 30 days, at 25 °C, over saturated solution of NaBr (RH ~ 56%). Films thickness was measured by hand-held micrometer (MICROMASTER Electronic Micrometer, Tesa Technology) for 8 random samples of each nanocomposite and no significant differences were observed (28.6 ± 4.4 μm; 26.4 ± 3.0 μm and 28.6 ± 2.4 μm for TPS, TPS/ZnONR-S and TPS/ZnONR-L, respectively).

2.3. Films characterizations

2.3.1. Morphological characterization

The cryogenic fracture surfaces of films were investigated with a field emission scanning electron microscopy (FE-SEM) Zeiss Supra 40. The fracture surface of the samples was sputter-coated with platinum (15 s, 0.06 mbar of Ar) and observed with an acceleration voltage of 5 kV.

2.3.2. UV–vis transmission

The UV–visible (UV–vis) transmission spectra of the films were recorded from 280 to 800 nm using a UV–vis spectrophotometer model UV-1650PC (Perkin Elmer).

2.3.3. X-ray diffraction (XRD)

The X-ray diffraction patterns of the films were measured with a Siemens D 5000 X-ray diffractometer. The X-ray generator tension and current were 40 kV and 30 mA, respectively. The radiation was Cu Kα with a wavelength of 1.54 Å. Data were collected in the range of $2\theta = 5–35°$ with a step size of 0.02°.

2.3.4. Contact angle, moisture content, solubility, water vapor permeability and roughness

To determine the hydrophobicity of the films, water contact angle (θ) measurements were performed using a microscope MicroView (USB Digital Microscope) coupled with image analysis software (Analysis Software 220 × 2.0 MP). A drop of distilled water (2 μL) was placed on the surface of each material. The methodology to calculate θ was based on the processing of images by determining the angle formed by the intersection of the liquid-solid interface (drop of water-surface of the film) and the liquid-vapor interface

(tangent on the boundary of the drop). Data presented are the mean of five independent determinations at different sites. Contact angles on each film surface were measured immediately after the addition of 2 μL deionized water.

Solubility of the films (S) in water was determined following Maizura, Fazilah, Norziah, & Karim (2007) with some modifications (Maizura et al., 2007). Pieces of film (1 × 1 cm) were cut from each film and dried at 50 °C for 24 h. Samples were weighed (m_{si}) with a resolution of 0.0001 g and placed in beakers with 50 mL deionized water. Then, samples were stirred with constant agitation for 24 h at room temperature. Film remnants were separated by filtration and dried at 50 °C to constant weight (m_{sf}). Samples were measured in three replicates and the percentage of total soluble matter was calculated as follows:

$$S = \frac{(m_{si} - m_{sf})}{m_{si}} \times 100 \quad (1)$$

Moisture content of the different films (MC) was determined using standard methods of analysis of the AOAC (1995). Pieces of each system (~0.5 g) were dried in an oven at 100 °C for 24 h. The percentage of moisture content was calculated as follow:

$$MC = \left(\frac{m_i - m_f}{m_i}\right) \times 100 \quad (2)$$

Where m_i is the initial weight and m_f is the dry weight of the samples.

Water vapor permeability (WVP) of the films was determined at room temperature using a modified ASTM E96-00 procedure (Famá et al., 2012). Samples were placed into circular acrylic cells containing $CaCl_2$ and located in desiccators at RH of ~70% and room temperature. Water vapor transport (WVT) was determined from the weight increase of the system from permeation, measuring over 24 h for 10 days. Finally, WVP were calculated as:

$$WVP = \frac{WVT \times e}{P_0 \times RH} \quad (3)$$

Where e is the film thickness and P_0 is the saturation vapor pressure of water at room temperature.

Roughness of the films surface (SR) was measured using a Sutronic 3+ rugosimeter (Taylor-Hobson). The data presented is the mean of 8 different measurements in different portions of the films.

2.3.5. Thermal analysis

Thermogravimetric (TGA) and differential thermal analysis (DTA) were carried out in a simultaneous TGA-DTA analyzer DTG-60 Shimadzu instrument. Approximately 5 mg of film samples were heated from room temperature to 500 °C at 10 °C/min, in a dry nitrogen atmosphere with flow rate of 30 mL/min.

2.3.6. Mechanical properties

Mechanical quasi-static tests were performed at room temperature using a Dynamic Mechanical Thermal Analyzer (DMTA IV, Rheometric Scientific). The tests were performed employing a strain rate fixed at a value of $1 \times 10^{-3}\ s^{-1}$ in a rectangular tension geometry following (ASTM, 2002) standard recommendations. Nominal stress (σ)–strain (ε) curves were obtained and Young's modulus, strength and strain at break values were determined. The reported results are the average of at least six independent experiments.

2.3.7. Biodegradation and bacterial growth inhibition

The biodegradation of films and bacterial growth inhibition in liquid medium were determined simultaneously, using the same film samples. Growth inhibition was estimated based on Tankhiwaleís work (Tankhiwale & Bajpai, 2012). Films were cut into squares (2 cm × 2 cm ~ 150 mg) and submerged in 20 mL phosphate saline buffer in a 25 mL beaker. The solution was inoculated with 200 μL of *E. coli* DH5α growth for 24 h in LB medium. The beakers were incubated in an orbital shaker for 24 h at 150 rpm and 37 °C. Bacterial growth in the beakers with different samples was determined by following the evolution of bacterial population with time. The optical density of samples taken at regular periods was measured at 620 nm. Bacterial population was estimated considering the approximation that an OD of 0.1 is equivalent to 10^8 UFC/ml of *E. coli*. Biodegradation of the film was determined by the loss weight after 24 h incubation. The remnant of the film was washed with distilled water, dried at 100 °C and weighed. The loss of water during drying at 100 °C and the mass loss by dissolution in the phosphate saline buffer were determined in control experiments and included in the calculation of biodegradability. The reported results are the average of five independent experiments. The concentration of zinc leached to the solution was determined by atomic absorption spectroscopy (SensAA dual, GBC Sci. equipment).

In another set of experiments, the beakers were illuminated from above with an incident radiation of 30 W/m^2 with a 300 W solar lamp (OSRAM, Ultravitalux) for 2 h before incubation to evaluate the photocatalytic effect of ZnO incorporated in the films. Bacterial growth and biodegradation were determined as explained above.

In different experiment, the evolution of film degradation was also followed by CO_2 production by *E. coli* with starch composites as the sole Carbon source. Films were cut into squares (2 cm × 2 cm ~ 150 mg film), and submerged in 20 mL phosphate saline buffer in a 100 mL reaction chamber. The solution was inoculated with 200 μL of *E. coli* DH5α growth for 24 h in LB medium. Sample chambers were placed in a water bath at 37 °C and connected to an automated and fully computerized closed-circuit Micro-Oxymax Respirometer System (Columbus Instruments) equipped with an expansion interface. Background CO_2 production by *E. coli* without composites was measured and subtracted from all experiments. All the experiments were run in duplicate.

Finally, the biodegradability of the films was evaluated in a vegetable compost to simulate the biodegradation of films in soils (Seligra, Medina Jaramillo, Famá, & Goyanes, 2016; Torres, Troncoso, Torres, Díaz, & Amaya, 2011) samples were cut in pieces of 1.2 cm × 1.2 cm. Vegetable compost was homogeneously distributed in plastic trays. Samples were buried under 4 cm of soil, in ambient temperature (~25 °C) and humidity (70–80%). Water was sprayed once a day to maintain the moisture of the compost. The films were removed at different times and vacuum dried at 50 °C for 24 h.

2.3.8. Data treatment and statistical analysis

Data were analyzed through two-way ANOVA and Tukey's Post-Hoc test at the 5% significance level ($p < 0.05$). Results were informed as the average and standard deviation.

3. Results and discussion

3.1. ZnONR characterization

Fig. 1 show FE-SEM micrographs and size distribution of ZnONR-S (A) and ZnONR-L (B), and XRD (C) of the composites. In both cases, the rods had hexagonal shape. Sample ZnONR-S (Fig. 1A) had a width of 15 ± 3 nm, and a length of 236 ± 52 nm, while sample ZnONR-L (Fig. 1B) had a width of 62 ± 17 nm and a length of 1027 ± 350 nm. However, the aspect ratio of both samples was very similar, being ~15.7 for ZnONR-S and ~16.5 for ZnONR-L. Both samples presented the wurzite type structure, according to the indexed JCPDS 36–1451, typically found in ZnO rods (Fig. 2C). ZnONR-L

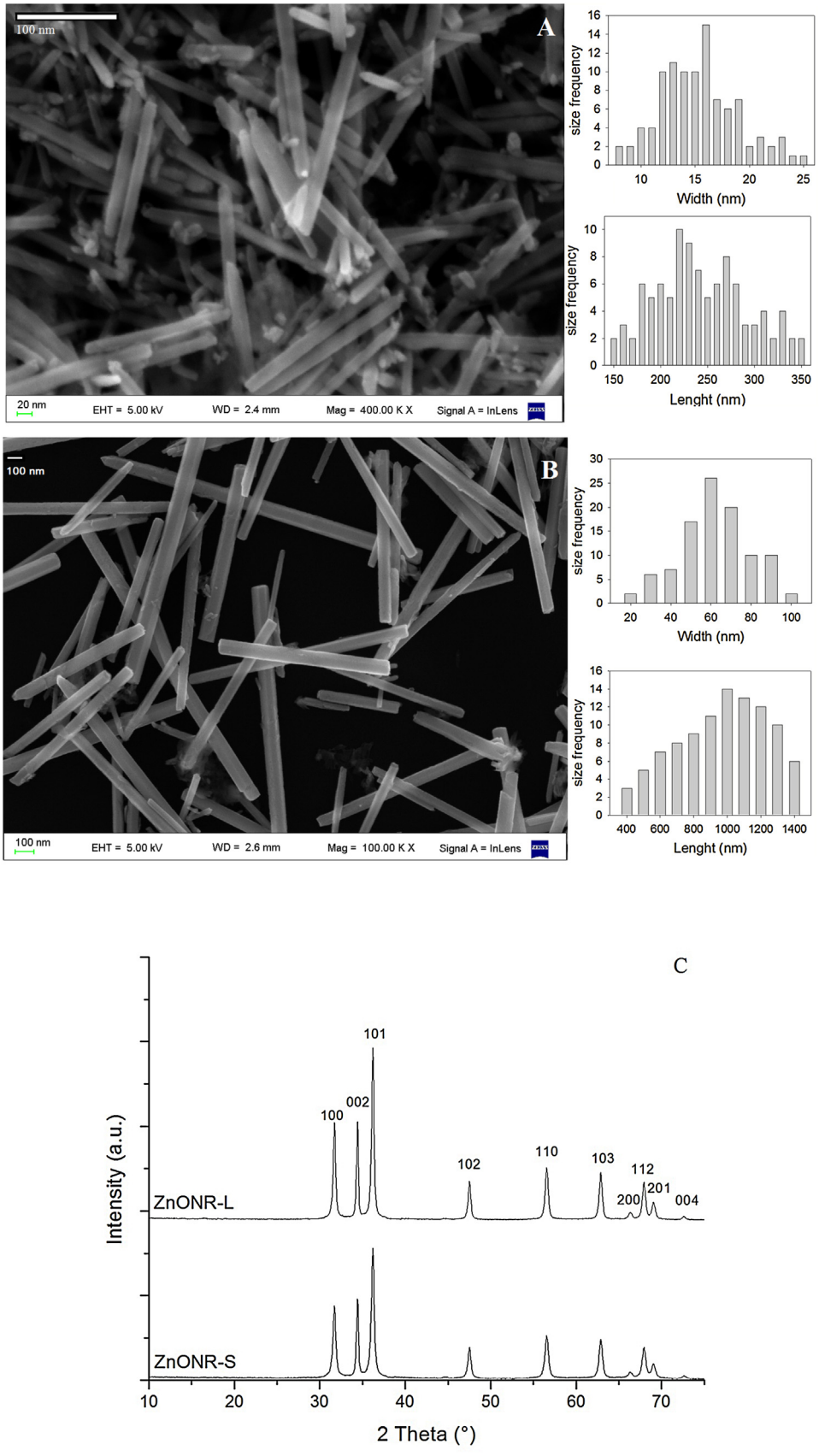

Fig. 1. SEM images and nanorods size distribution of ZnONR-S (a) and ZnONR-L (b), and XRD of ZnONR-S and ZnONR-L nanorods.

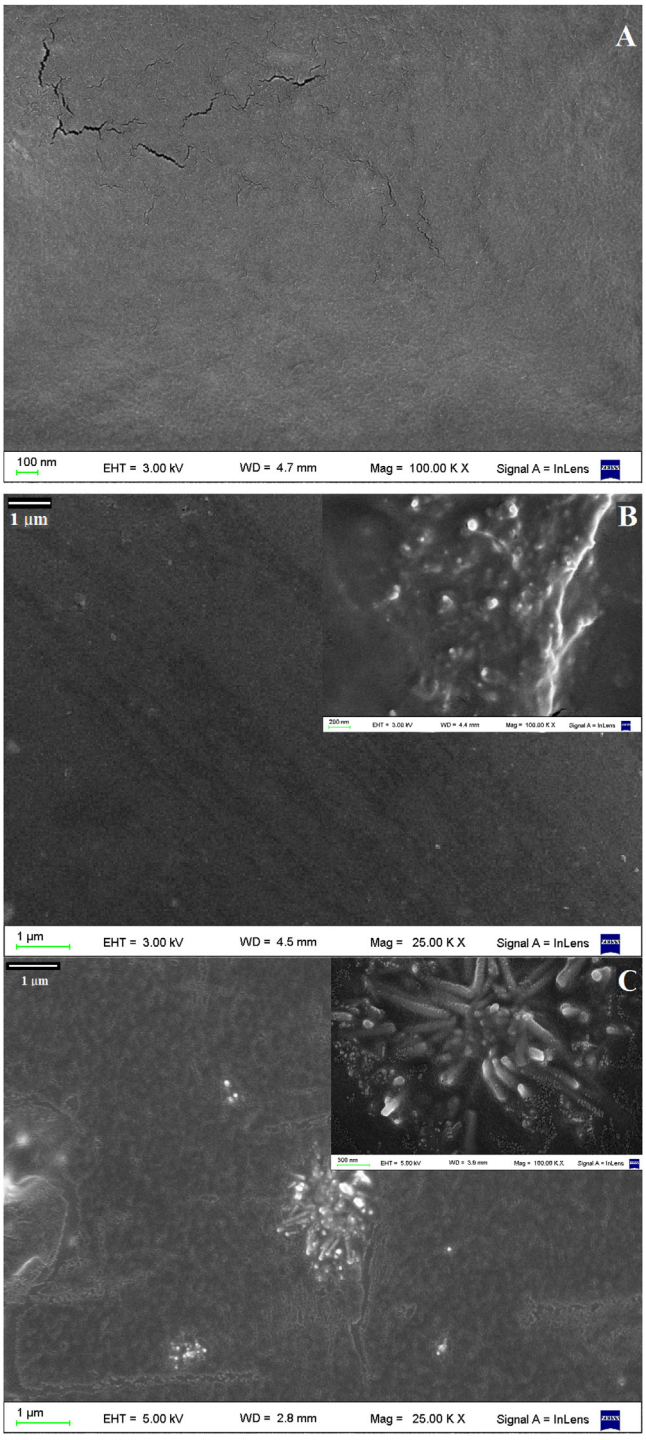

Fig. 2. SEM images of cryogenic fracture of TPS matrix (A), TPS with 1 wt.% of ZnONR-S (B) and ZnONR-L (C).

rods presented narrower and more intense diffraction peaks than ZnONR-S, indicating that the rods with larger size were more crystalline than the ones with the smaller size. The Full Width at Half Maximum (FWHM) of the (002) peak was smaller than those corresponding to the (100) and (101) peaks, indicating a net growth in the ⟨0001⟩ direction in both samples. The relationship between the (002) polar plane intensity and (100) non polar plane intensity (Li et al., 2008) did not present significant differences in both samples ($I_{(002)}/I_{(100)} \sim 1.0$). There were no significant differences in Z potential between both sizes of ZnONR in the range of pH

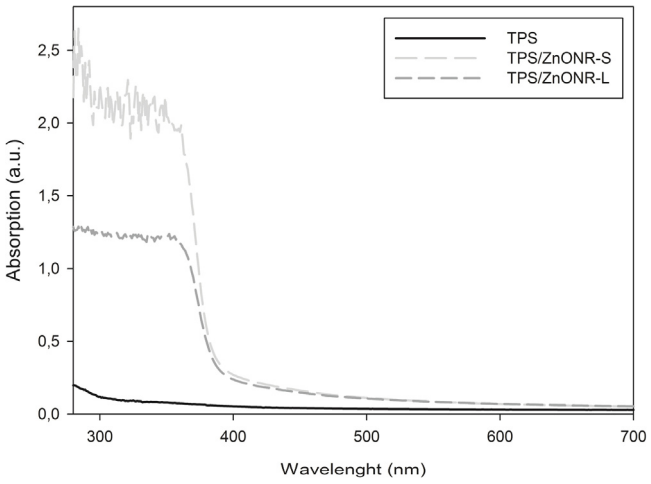

Fig. 3. Light absorption of TPS, TPS/ZnONR-S and TPS/ZnONR-L films.

studied (Supplementary Fig. 2). Around neutral pH, rods were positively charged, and at pH higher than 9 both rods are negatively charged. ZnONR-S and ZnONR-L had an isoelectric point of 8.75 and 8.87 respectively. This result suggests that ZnONR could be well dispersed in water before their incorporation to the starch suspension. Other authors reported similar results for ZnO nanoparticle suspensions in water, with positive values near neutral pH and isoelectric point around 9.4 (L. Zhang, Jiang, Ding, Povey, & York, 2007; Y. Zhang, Chen, Westerhoff, & Crittenden, 2009).

3.2. Starch/ZnO—NR nanocomposites

3.2.1. Morphological characterization

In Fig. 2 SEM images of cryogenic fracture surface of TPS (A), and composites TPS/ZnONR-S (B) and TPS/ZnONR-L (C) are shown. As can be seen, the rods conserved their hexagonal shape after been incorporated in the TPS matrix (Fig. 2B and C). Besides, adhesion between the ZnONR and the matrix, without the presence of holes in the interface, was observed. However smaller ZnONR-S were homogeneously distributed on the TPS matrix, whilst higher size ZnONR-L formed agglomerates on the TPS matrix.

3.2.2. UV–vis absorption spectra

Fig. 3 shows the UV–vis absorption spectra corresponding to the different composites. TPS/ZnONR-S composite had a higher UV absorption (around 70%) compared with the value of TPS/ZnONR-L, demonstrating that ZnO nanorods size has a key role in UV shielding. Both composites also presented increases in UV absorption respected to the matrix in all the studied range. Nafchi et al. (2013) found in sago starch composites containing 1 wt.% ZnO nanorods of 200–700 nm length and 40–100 nm diameter absorption values in the UV range that are between the values reported in this work for TPS/ZnONR composites (Nafchi et al., 2013). The authors increased the concentration of ZnO rods in the composites to increase UV absorption. According to our results it is possible to increase UV absorption, without increasing ZnO content, by simply resizing the nanorods maintaining its aspect relationship, thus avoiding increments in the cost of the material and abiding to legislation limits (EFSA Panel on Food Contact Materials, 2016). This increase in UV absorption could be consequence of a higher surface-to-volume ratio of the smaller ZnONR-S, which leads to higher oxygen vacancies and intrinsic defects (Liao et al., 2007).

The figure also shows that both types of rods incorporated in the starch matrix had very similar band gap. ZnONR-S confined in the starch matrix showed a band gap of 3.34 eV and ZnONR-L a band gap of 3.37 eV. These results suggest that the films filled with ZnONR-S

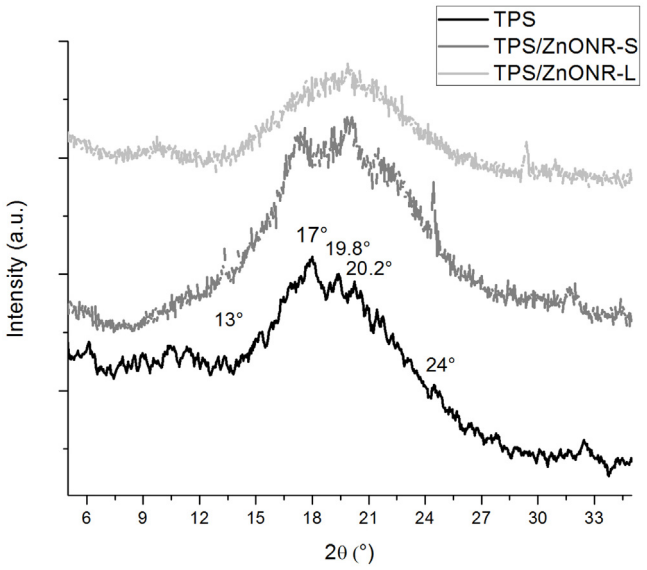

Fig. 4. XRD patterns of TPS, TPS/ZnONR-S and TPS/ZnONR-L films.

could be used as an UV-shielding agent in plasticized tapioca starch films.

3.2.3. X-Ray diffraction pattern (XRD)

Fig. 4 shows XRD patterns of the films measurement at 30 days of storage. As can be seen, it is very significant the effect of the filler size in the crystallinity of the composites. The thermoplastic starch matrix presented the typical B-V type crystalline structure with peaks at $2\theta = 13^\circ$, 17°, 19.8°, 20.2° and 24°. The presence of this structure was associated with a retrogradation process resulting from the storage of the samples at 56% RH (Wynne-Jones & Blanshard, 1986). The incorporation of ZnONR-S produced the intensification of the relative intensity of the peaks at $2\theta = 13^\circ$, 20.2° and 24°, corresponding to V-type starch structure, with respect to the peaks at $2\theta = 17^\circ$ and 19.8°, associated with the B-type starch structure. However, the addition of ZnONR-L produced practically amorphous composite. It is well known that amylose adopts a left handed single helix V-type crystalline structure in the presence of complexing agents, such as glycerol. The V-type lattice has a relatively large cavity, which is thought to contain the complexing agent (van Soest, Hulleman, De Wit, & Vliegenthart, 1996). Other authors reported that high glycerol content induces the formation of the single helix structure, but limits that of B-type double helix structure (Shi et al., 2007). These results indicated that, in the presence of ZnONR-S, the way in which glycerol interacts with amylose notably changed with respect to TPS films. It seems that glycerol is more available to interact with amylose in the presence of ZnONR-S. This phenomenon may be consequence of the relatively lower hydrophilicity of ZnONR-S with respect to amylose, because the exposed planes are the non polar 100 and 101 (Mclaren, Valdes-Solis, Li, & Tsang, 2009). Besides, ZnONR-S could act as nuclei centers, inducing crystallization in a V-type structure. The amorphous structure induced by the incorporation of ZnONR-L indicated that the highest rod size prevented starch retrogradation during storage. ZnONR-L could interact with several starch molecules, generating a network structure that inhibits crystallization from retrogradation leading to increased amount of free glycerol to act as plasticizer. Mathew, Thielemans, and Dufresne (2008) proposed a similar mechanism for Tunicin whiskers reinforced starch films with sorbitol as plasticizer (Mathew et al., 2008). Wu & Chen (2006) also proposed a similar mechanism for the retardation of the crystallization of poly (ε-coprolactone) with the incorporation of a high concentration of carbon nanotubes (Wu & Chen, 2006). Siqueira, Bras, and Dufresne (2008) also found that the nature of the filler influences the crystallinity of the film in polycaprolactone films (Siqueira et al., 2008). Using cellulose microfibrills resulted in a more amorphous composite than using cellulose nanowhiskers. The authors also proposed that the microfibrills confines the polymeric matrix and retardates the composite crystallization.

3.2.4. Films hydrophilicity

Table 1 shows the contact angle (θ), moisture content (MC), water solubility (S), water vapor permeability (WVP) and surface rugosity (R_a) of the three different films. It is clear that the incorporation of ZnONR to the matrix produced a notable change in the studied properties, but the magnitude of the change was strongly influenced by the size of the ZnONR. The difference in contact angle between composites with ZnONR-L or ZnONR-S was 12%, being higher in the case of ZnONR-L indicating a more hydrophobic material. The difference in contact angle may be related to the surface roughness and/or the availability of OH on the surface of the films. However, as shown in Table 1, there were no significant differences in the roughness of the air dried face of the films. This result indicated that the difference between the contact angles may be related with OH availability as consequence of different starch packing as was indicated in XRD analysis. The diminution in moisture content and solubility can also be related with the increment in hydrophobicity.

The size of the ZnONR also affected the WVP. Data shown in Table 1 indicate that WVP was 11% lower in the case of TPS/ZnONR-L with respect to TPS/ZnONR-S. For a fixed weight percentage of filler, the water transport through the composite is a function of the filler's chemical composition and geometric-hindered factor, which is a function of filler geometry and orientation angle (Sorrentino, Tortora, & Vittoria, 2006). The different WVP values determined for TPS/ZnONR-L and TPS/ZnONR-S could be consequence of filler orientation in the matrix or the packing arrangement of starch molecules in the composite (as can be deduced from XRD pattern shown in Fig. 4).

3.2.5. Thermal analysis

Fig. 5A and B show the TGA and DTA of the composites respectively. In all the cases there is a loss of mass in the range 25–110 °C, which corresponds to an endothermic process centered at 100 °C, that can be associated with water evaporation. At higher temperatures, samples shows two main stages typically observed in thermoplastic starch based films (García, Famá, Dufresne, Aranguren, & Goyanes, 2009; Medina Jaramillo, González Seligra, Goyanes, Bernal, & Famá, 2015), that are associated to the glycerol rich phase (180–280 °C) and starch rich phase decomposition (280–350 °C). As can be observed in TGA curves (Fig. 5A), these processes are different in all samples. Although both composites began these degradation processes at lower temperatures than the matrix, it is notorious that the incorporation of larger ZnONR-L led to a more marked behavior, showing the beginning of glycerol degradation at ~150 °C. Besides, TPS/ZnONR-L presented two close peaks in the DTA curve (Fig. 5B), centered in 265 °C and 285 °C, and a third peak in 320 °C. These phenomena may be related with the size effect of ZnONR on the structure of the starch. In the presence of larger ZnONR-L the composite is non crystalline, the decrease at the beginning of thermal decomposition suggests that in this case glycerol is even less confined than in the other cases. As it was discussed above, the presence of ZnONR-S led to an enrichment of the V-type structure (see Fig. 4). This simple helix structure is less compact than the double helix B-type, containing glycerol in cavities (Le Bail et al., 1999), causing also a decrease at the beginning of the thermal decomposition of TPS/ZnONR-S respect to the matrix due to the loss of glycerol. It is notorious that the amorphous nature

Table 1
Contact angle (θ), moisture content (MC), water solubility (S), surface roughness (SR) and water vapor permeability (WVP) of TPS, TPS/ZnONR-S and TPS/ZnONR-L.

	Θ (°)	MC (%)	S (%)	SR (R_a)	WVP (10^{-10} g m^{-1} seg^{-1} Pa^{-1})
TPS	53 ± 3^a	23 ± 2^a	23 ± 2^a	1.5 ± 0.5^a	6.8 ± 0.4^a
TPS/ZnONR-S	65 ± 3^b	19 ± 2^b	16 ± 2^b	1.9 ± 0.4^a	5.3 ± 0.1^b
TPS/ZnONR-L	73 ± 1^c	16 ± 1^c	8 ± 1^c	2.3 ± 0.4^a	4.7 ± 0.4^c

Different letters indicate statistical difference ($p < 0.05$) by Tukey's Post-Hoc test.

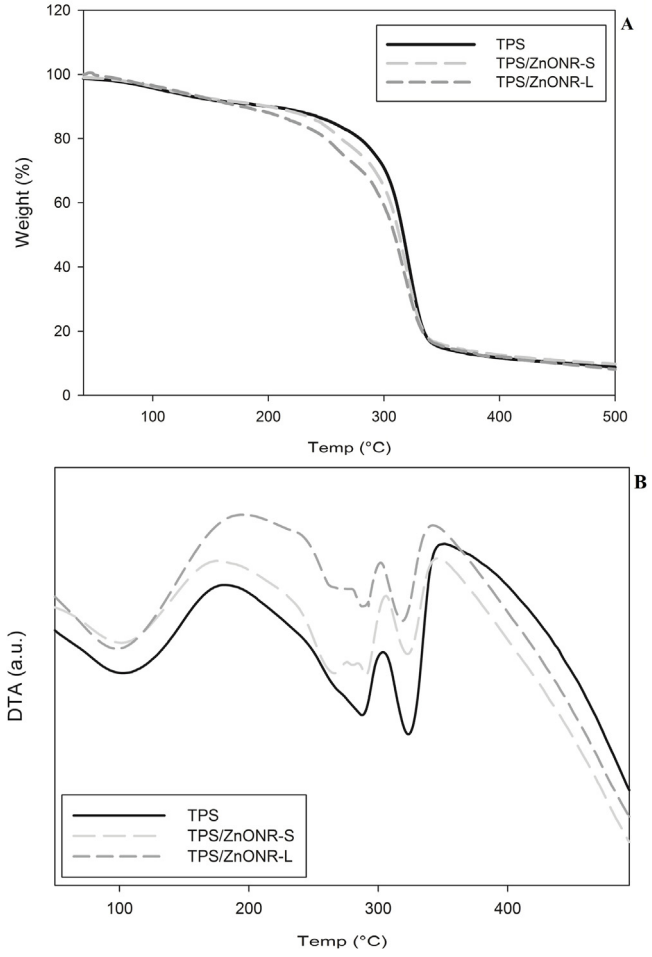

Fig. 5. TGA (A) and DTA (B) of TPS, TPS/ZnONR-S and TPS/ZnONR-L films.

Table 2
Mechanical properties of the composites.

	E (MPa)	ε_b (%)	σ_b (MPa)
TPS	5.7 ± 0.1^a	46 ± 3^a	3.6 ± 0.2^a
TPS/ZnONR-S	4.1 ± 0.4^b	50 ± 5^{ab}	3.2 ± 0.2^b
TPS/ZnONR-L	3.6 ± 0.3^b	58 ± 6^b	2.8 ± 0.2^c

Different letters indicate statistical difference ($p < 0.05$) by Tukey's Post-Hoc test.

of the TPS/ZnONR-L composite predominated in the beginning of the degradation versus the V-type structure TPS/ZnONR-S.

3.2.6. Mechanical characterization

Young's modulus (E), strain at break (ε_b) and stress at break (σ_b) of the matrix and composites are shown in Table 2 (typical stress-strain curves can be seen in Supplementary Fig. 3). In both composites a tendency to increase the strain at break and to decrease the Young's modulus and stress at break were observed. The tendency observed in mechanical properties could be a consequence of available plasticizer. In the case of the films presented in these work, water and glycerol could act as plasticizer. As shown in the TGA (Fig. 5A), the addition of ZnONR-L led to a composite with more available glycerol, and consequently more effective as plasticizer, increasing ε_b, and decreasing E and σ_b. The results of moisture content shows that water content decreased, suggesting a diminution of ε_b and increment of E and σ_b. Taking into account both results, the tendency in the mechanical properties values suggests that the increased glycerol mobility, has a greater effect than moisture decrease.

Another factor that may affect mechanical properties is the packing of the starch molecules. TPS/ZnONR-L was an amorphous composite while TPS/ZnONR-S displayed a XRD pattern showing the presence of the V-B phases with a higher proportion of the V fraction.

3.2.7. Antimicrobial activity

Table 3 shows biodegradation of composites and bacterial growth inhibition in solution after 24 h. The addition of ZnONR greatly reduced the biodegradation of films and the final population of *E. coli* in the liquid suspension. The only carbon source for bacterial growth was the film itself. ZnONR-S showed a significant more efficient bacterial growth inhibition and protected more the composite from biodegradation than ZnONR-L. After 24 h incubation, CFU in TPS/ZnONR-S system was 57% lower than in the case of TPS/ZnONR-L.

Irradiating the suspension with UV light for 2 h before incubation enhanced the antibacterial effect of all films. UV light has an intrinsic antibacterial effect, and reduces the final number of *E. coli*, even on TPS film. By exposing the TPS films with UV light during 2 h just before incubation, CFU were reduced by 32% with respect to the non-illuminated sample. In the case of TPS/ZnONR-S the reduction was 85% while for TPS/ZnONR-L was 69%. Incorporation of smaller ZnONR-S into the TPS matrix in darkness produced similar inhibitory effect than UV illuminated larger nanorods.

The Zn^{2+} leached to the solution per unit of mass of each composite was slightly smaller for the composite with the smaller nanorods, with no significant difference between irradiated and non-irradiated samples. In the absence of bacteria and in darkness, the release of Zn^{2+} was higher in the composite with the higher size ZnO rods. TPS/ZnONR-L released 0.40 mg/L (8.0 mg Zn^{2+}/kg film) while for TPS/ZnONR-S composite it was 0.34 mg/L (6.8 mg Zn^{2+}/kg film).

Particle dissolution to ionic zinc and particle-induced generation of reactive oxygen species (ROS) represent the primary modes of action for ZnO nanoparticles toxicity (Ma, Williams, and Diamond (2013) and references therein). Both modes are likely present in the cases studied in this work. It is remarkable that the concentrations of Zn^{2+} in solution were within the range for optimal bacterial growth (Sugarman, 1983) and were lower than the maximum allowed for drinking water and protection of aquatic life according to EPA (EPA 78/659/EEC). However, bacteria interacted with the starch matrix dissolving and fractionating it; consequently, local concentrations of Zn^{2+} higher than those measured in solution cannot be disregarded. Due to the activity of bacteria on the composite films, ZnONR became exposed at the surface and likely interacted with the bacteria membrane affecting its integrity by the action of ROS produced at the ZnO surface.

Table 3
Biodegradation, bacterial growth inhibition and Zn^{2+} release of TPS, TPS/ZnONR-S and TPS/ZnONR-L films in darkness and with 2 h of UV light before incubation.

	In Darkness			2 h UV Light before incubation		
	% Biodeg	CFU/ml ($\times 10^9$)	Zn^{2+} (mg/kg)	% Biodeg	CFU/ml ($\times 10^9$)	Zn^{2+} (mg/kg)
TPS	52 ± 2^a	8.3 ± 0.2^a	ND	34 ± 2^a	5.6 ± 0.1^a	ND
TPS/ZnONR-S	21 ± 1^b	2.6 ± 0.1^b	4.7 ± 0.2^a	15 ± 1^b	1.5 ± 0.1^b	4.9 ± 0.4^a
TPS/ZnONR-L	24 ± 1^c	4.6 ± 0.3^c	5.1 ± 0.7^a	19 ± 1^c	2.7 ± 0.1^c	5.4 ± 0.6^a

Different letters indicate statistical difference ($p < 0.05$) by Tukey's Post-Hoc test.

(see (Applerot et al., 2009) for details about the bactericidal mechanisms of ZnO nanoparticles via ROS generation). The size of the ZnO nanoparticles has an important role because the smaller the particles, faster will release Zn^{2+} to the solution and higher will be ROS production (which takes place at the surface of the nanoparticles). This phenomenon may explain the higher bacterial growth inhibitory effect of smaller ZnONR with respect to larger ones. Other authors also observed that smaller size rods have higher antibacterial activity than higher size rods for *E. coli* in the dark (Nair et al., 2009).

It is well established in the literature that ZnO has a photocatalityc oxidation activity producing ROS, especially $OH^{\bullet -}$ and H_2O_2. This phenomenon explains the enhanced bacterial growth inhibition presented by the composite films under UV illumination. The composite containing the smaller nanorods presented higher UV adsorption, as shown in Fig. 3. The adsorption of more UV light could lead to a higher production of ROS and consequently a higher inhibitory effect as shown in Table 3.

The specific production of CO_2 by bacteria in PBS buffer suspension with the starch composites as the sole Carbon source was evaluated (Supplementary Fig. 4). After a 5 h lag period, bacteria started to degrade all the composites. TPS showed the highest initial biodegradation velocity by *E. coli*. Both composites with ZnO showed similar initial velocities, however, the incorporation of ZnONR-S reduced the final extent of liberated CO_2 of the composite compared to TPS/ZnONR-L. Taking in consideration the results obtained by bacterial count (Table 3), the decrease of CO_2 production was probably a consequence of a reduction in the bacterial population. Another factor that could be affecting the biodegradability of the composites is the decrease of the solubility and wettability because of ZnONR incorporation (Table 2).

Supplementary Fig. 5 shows the macroscopic appearance of films buried in vegetable compost at different time intervals. Independently of the addition or size of ZnONR, all films showed significant biodegradation after 30 days. At 6 days, the TPS matrix showed significant signs of biodegradation. Composites with largest ZnONR also began to degrade while in TPS/ZnONR-S only slight bacterial and fungal growth on the surface of the films was observed. After 13 days, the composite with ZnONR-L showed higher signs of degradation; however, the composite with the smaller size of rods still resisted biodegradation. This behavior occurred until the 19th day.

Other authors indicated that using ZnO as crosslink in PVA/starch films delayed the initial biodegradation of films as a consequence of less OH free groups and decreased moisture adsorption (Maiti, Ray, & Mitra, 2012). However, our results indicated that, even though higher size rods produced a more hydrophobic film, the effect of smaller size nanorods in bacterial growth inhibition was more important in film biodegradation retardation.

4. Conclusions

The size of ZnO nanorods, for a given aspect ratio and physicochemical properties, determined the characteristics of thermoplastic starch based composites. It is remarkable that several properties of the composite can be tuned by changing the size of the nanorods without modify the wt.% of filler. Depending on the property to be enhanced, small or large ZnONR can be used. Smaller size rods (ZnONR-S) have greater bactericidal effect than larger rods (ZnONR-L), being the amount of Zn^{2+} released from the composite within the permitted limits for food contact materials independently of the rod size. The addition of smaller size rods also produces a slight decrease in the degradation process of the film in soil and the best results as UV shielding. The use of larger nanorods is more effective to increase contact angle and decrease moisture content, water solubility and water vapor permeability. The higher size of the filler also magnifies the differences in the mechanical properties of the composite with respect to the matrix, showing the highest strain at break and lowest Young's modulus and strength at break.

Finally, it is interesting to remark that all these effects are linked to the microstructure of the films, which is strongly affected by the size of the nanorods. While small nanorods maintain a B-V type crystalline structure, intensifying the peaks corresponding to V-type starch structure, larger nanorods induce the formation of an amorphous structure, preventing starch retrogradation during storage.

These results suggest that larger rods could be incorporated in composite materials for improving its mechanical and thermal properties, whilst shorter rods could be incorporated for potential food packaging materials with better UV shielding and antimicrobial properties.

Acknowledgements

The authors wish to acknowledge the support and collaboration of the following organizations: CONICET (PIP 2014–2016, 11220120100508CO), University of Buenos Aires (UBACYT 2014–2017, 20020130100495BA), ANPCyT (PICT-2012-1093). SG, RC and LF are members of CONICET. The authors wish to thank the fellowship granted to L.G. by CONICET.

Appendix A. Supplementary data

Supplementary data associated with this article can be found, in the online version, at http://dx.doi.org/10.1016/j.carbpol.2016.11.041.

References

ASTM D.-. (2002). *Annual book of ASTM*. West Conshohocken, USA: American Society for Testing and Materials.
Alebooyeh, R., Nafchi, A., & Jokr, M. (2012). The effects of ZnO nanorods on the characteristics of sago starch biodegradable films. *Journal of Chemical Health Risks*, *2*(4)
Angles, M. N., & Dufresne, A. (2001). Plasticized starch/tunicin whiskers nanocomposite materials. 2. Mechanical behavior. *Macromolecules*, *34*(9), 2921–2931.
AOAC, 1995 Official methods of analysis Association of Official Analytical Chemists, Washington, DC (1995).
Applerot, G., Lipovsky, A., Dror, R., Perkas, N., Nitzan, Y., Lubart, R., & Gedanken, A. (2009). Enhanced antibacterial activity of nanocrystalline ZnO due to increased ROS mediated cell injury. *Advanced Functional Materials*, *19*(6), 842–852.
Arfat, Y. A., Benjakul, S., Prodpran, T., Sumpavapol, P., & Songtipya, P. (2014). Properties and antimicrobial activity of fish protein isolate/fish skin gelatin

film containing basil leaf essential oil and zinc oxide nanoparticles. *Food Hydrocolloids*, *41*, 265–273.
Arora, A., & Padua, G. W. (2010). Review: Nanocomposites in food packaging. *Journal of Food Science*, *75*(1), R43–R49.
Bertuzzi, M. A., Castro Vidaurre, E. F., Armada, M., & Gottifredi, J. C. (2007). Water vapor permeability of edible starch based films. *Journal of Food Engineering*, *80*(3), 972–978.
Cano, A., Fortunati, E., Cháfer, M., Kenny, J. M., Chiralt, A., & González-Martínez, C. (2015). Properties and ageing behaviour of pea starch films as affected by blend with poly(vinyl alcohol). *Food Hydrocolloids*, *48*, 84–93.
Chen, Y., Liu, C., Chang, P. R., Anderson, D. P., & Huneault, M. A. (2009). Pea starch-based composite films with pea hull fibers and pea hull fiber-derived nanowhiskers. *Polymer Engineering & Science*, *49*(2), 369–378.
Chen, Y., Liu, C., Chang, P. R., Cao, X., & Anderson, D. P. (2009). Bionanocomposites based on pea starch and cellulose nanowhiskers hydrolyzed from pea hull fibre: Effect of hydrolysis time. *Carbohydrate Polymers*, *76*(4), 607–615.
Chen, Y. W., Qiao, Q., Liu, Y. C., & Yang, G. L. (2009). Size-controlled synthesis and optical properties of small-sized ZnO nanorods. *The Journal of Physical Chemistry C*, *113*(18), 7497–7502.
de Azeredo, H. M. C., Mattoso, L. H. C., & McHugh, T. H. (2011). *Nanocomposites in food packaging–A review*. INTECH Open Access Publisher.
EFSA Panel on Food Contact Materials, E., Flavourings and Processing Aids. (2016). Scientific opinion on the safety assessment of the substance zinc oxide, nanoparticles, for use in food contact materials. *EFSA Journal*, *14*(3), 8.
Emamifar, A., Kadivar, M., Shahedi, M., & Soleimanian-Zad, S. (2010). Evaluation of nanocomposite packaging containing Ag and ZnO on shelf life of fresh orange juice. *Innovative Food Science & Emerging Technologies*, *11*(4), 742–748.
Famá, L., Bittante, A. M. B. Q., Sobral, P. J. A., Goyanes, S., & Gerschenson, L. N. (2010). Garlic powder and wheat bran as fillers: Their effect on the physicochemical properties of edible biocomposites. *Materials Science and Engineering: C*, *30*(6), 853–859.
Famá, L., Rojo, P. G., Bernal, C., & Goyanes, S. (2012). Biodegradable starch based nanocomposites with low water vapor permeability and high storage modulus. *Carbohydrate Polymers*, *87*(3), 1989–1993.
García, N. L., Famá, L., Dufresne, A., Aranguren, M., & Goyanes, S. (2009). A comparison between the physico-chemical properties of tuber and cereal starches. *Food Research International*, *42*(8), 976–982.
Gutiérrez, T. J., Tapia, M. S., Pérez, E., & Famá, L. (2015). Structural and mechanical properties of edible films made from native and modified cush–cush yam and cassava starch. *Food Hydrocolloids*, *45*, 211–217.
Jiménez, A., Fabra, M. J., Talens, P., & Chiralt, A. (2012). Edible and biodegradable starch films: A review. *Food and Bioprocess Technology*, *5*(6), 2058–2076.
Kanmani, P., & Rhim, J.-W. (2014). Properties and characterization of bionanocomposite films prepared with various biopolymers and ZnO nanoparticles. *Carbohydrate Polymers*, *106*, 190–199.
Laohakunjit, N., & Noomhorm, A. (2004). Effect of plasticizers on mechanical and barrier properties of rice starch film. *Starch – Stärke*, *56*(8), 348–356.
Le Bail, P., Bizot, H., Ollivon, M., Keller, G., Bourgaux, C., & Buléon, A. (1999). Monitoring the crystallization of amylose–lipid complexes during maize starch melting by synchrotron x-ray diffraction. *Biopolymers*, *50*(1), 99–110.
Li, G. R., Hu, T., Pan, G. L., Yan, T. Y., Gao, X. P., & Zhu, H. Y. (2008). Morphology-function relationship of ZnO: Polar planes, oxygen vacancies, and activity. *The Journal of Physical Chemistry C*, *112*(31), 11859–11864.
Liao, L., Lu, H. B., Li, J. C., He, H., Wang, D. F., Fu, D. J., . . . & Zhang, W. F. (2007). Size dependence of gas sensitivity of ZnO nanorods. *The Journal of Physical Chemistry C*, *111*(5), 1900–1903.
Ma, H., Williams, P. L., & Diamond, S. A. (2013). Ecotoxicity of manufactured ZnO nanoparticles–a review. *Environmental Pollution*, *172*, 76–85.
Maiti, S., Ray, D., & Mitra, D. (2012). Role of crosslinker on the biodegradation behavior of starch/polyvinylalcohol blend films. *Journal of Polymers and the Environment*, *20*(3), 749–759.
Maizura, M., Fazilah, A., Norziah, M. H., & Karim, A. A. (2007). Antibacterial activity and mechanical properties of partially hydrolyzed sago starch-alginate edible film containing lemongrass oil. *Journal of Food Science*, *72*(6), C324–C330.
Mathew, A. P., Thielemans, W., & Dufresne, A. (2008). Mechanical properties of nanocomposites from sorbitol plasticized starch and tunicin whiskers. *Journal of Applied Polymer Science*, *109*(6), 4065–4074.
Mclaren, A., Valdes-Solis, T., Li, G., & Tsang, S. C. (2009). Shape and size effects of ZnO nanocrystals on photocatalytic activity. *Journal of the American Chemical Society*, *131*(35), 12540–12541.
Medina Jaramillo, C., González Seligra, P., Goyanes, S., Bernal, C., & Famá, L. (2015). Biofilms based on cassava starch containing extract of yerba mate as antioxidant and plasticizer. *Starch – Stärke*, *67*(9–10), 780–789.
Morales, N. J., Candal, R., Famá, L., Goyanes, S., & Rubiolo, G. H. (2015). Improving the physical properties of starch using a new kind of water dispersible nano-hybrid reinforcement. *Carbohydrate Polymers*, *127*, 291–299.
Morsy, M. K., Khalaf, H. H., Sharoba, A. M., El-Tanahi, H. H., & Cutter, C. N. (2014). Incorporation of essential oils and nanoparticles in pullulan films to control foodborne pathogens on meat and poultry products. *Journal of Food Science*, *79*(4), M675–M684.
Nafchi, A. M., Alias, A. K., Mahmud, S., & Robal, M. (2012). Antimicrobial, rheological, and physicochemical properties of sago starch films filled with nanorod-rich zinc oxide. *Journal of Food Engineering*, *113*(4), 511–519.
Nafchi, A. M., Nassiri, R., Sheibani, S., Ariffin, F., & Karim, A. (2013). Preparation and characterization of bionanocomposite films filled with nanorod-rich zinc oxide. *Carbohydrate Polymers*, *96*(1), 233–239.
Nair, S., Sasidharan, A., Rani, V. D., Menon, D., Nair, S., Manzoor, K., & Raina, S. (2009). Role of size scale of ZnO nanoparticles and microparticles on toxicity toward bacteria and osteoblast cancer cells. *Journal of Materials Science: Materials in Medicine*, *20*(1), 235–241.
Pantani, R., Gorrasi, G., Vigliotta, G., Murariu, M., & Dubois, P. (2013). PLA-ZnO nanocomposite films: Water vapor barrier properties and specific end-use characteristics. *European Polymer Journal*, *49*(11), 3471–3482.
Seligra, P. G., Medina Jaramillo, C., Famá, L., & Goyanes, S. (2016). Biodegradable and non-retrogradable eco-films based on starch-glycerol with citric acid as crosslinking agent. *Carbohydrate Polymers*, *138*, 66–74.
Shankar, S., Teng, X., Li, G., & Rhim, J.-W. (2015). Preparation, characterization and antimicrobial activity of gelatin/ZnO nanocomposite films. *Food Hydrocolloids*, *45*, 264–271.
Shi, R., Liu, Q., Ding, T., Han, Y., Zhang, L., Chen, D., & Tian, W. (2007). Ageing of soft thermoplastic starch with high glycerol content. *Journal of Applied Polymer Science*, *103*(1), 574–586.
Siracusa, V., Rocculi, P., Romani, S., & Rosa, M. D. (2008). Biodegradable polymers for food packaging: A review. *Trends in Food Science & Technology*, *19*(12), 634–643.
Siqueira, G., Bras, J., & Dufresne, A. (2008). Cellulose whiskers versus microfibrils: influence of the nature of the nanoparticle and its surface functionalization on the thermal and mechanical properties of nanocomposites. *Biomacromolecules*, *10*(2), 425–432.
Sorrentino, A., Tortora, M., & Vittoria, V. (2006). Diffusion behavior in polymer?clay nanocomposites. *Journal of Polymer Science Part B: Polymer Physics*, *44*(2), 265–274.
Soykeabkaew, N., Supaphol, P., & Rujiravanit, R. (2004). Preparation and characterization of jute- and flax-reinforced starch-based composite foams. *Carbohydrate Polymers*, *58*(1), 53–63.
Sugarman, B. (1983). Zinc and infection. *Review of Infectious Diseases*, *5*(1), 137–147.
Tankhiwale, R., & Bajpai, S. K. (2012). Preparation, characterization and antibacterial applications of ZnO-nanoparticles coated polyethylene films for food packaging. *Colloids and Surfaces B: Biointerfaces*, *90*, 16–20.
Torres, F., Troncoso, O., Torres, C., Díaz, D., & Amaya, E. (2011). Biodegradability and mechanical properties of starch films from Andean crops. *International Journal of Biological Macromolecules*, *48*(4), 603–606.
van Soest, J. J., Hulleman, S., De Wit, D., & Vliegenthart, J. (1996). Crystallinity in starch bioplastics. *Industrial Crops and Products*, *5*(1), 11–22.
Vieira, M. G. A., da Silva, M. A., dos Santos, L. O., & Beppu, M. M. (2011). Natural-based plasticizers and biopolymer films: A review. *European Polymer Journal*, *47*(3), 254–263.
Wang, J., Kulkarni, A. J., Ke, F. J., Bai, Y. L., & Zhou, M. (2008). Novel mechanical behavior of ZnO nanorods. *Computer Methods in Applied Mechanics and Engineering*, *197*(41–42), 3182–3189.
Wu, T.-M., & Chen, E.-C. (2006). Isothermal and nonisothermal crystallization kinetics of poly (ε-caprolactone)/multi-walled carbon nanotube composites. *Polymer Engineering & Science*, *46*(9), 1309–1317.
Wynne-Jones, S., & Blanshard, J. M. V. (1986). Hydration studies of wheat starch, amylopectin, amylose gels and bread by proton magnetic resonance. *Carbohydrate Polymers*, *6*(4), 289–306.
Xie, F., Pollet, E., Halley, P. J., & Avérous, L. (2013). Starch-based nano-biocomposites. *Progress in Polymer Science*, *38*(10–11), 1590–1628.
Yi, S.-H., Choi, S.-K., Jang, J.-M., Kim, J.-A., & Jung, W.-G. (2007). Low-temperature growth of ZnO nanorods by chemical bath deposition. *Journal of Colloid and Interface Science*, *313*(2), 705–710.
Zhang, L., Jiang, Y., Ding, Y., Povey, M., & York, D. (2007). Investigation into the antibacterial behaviour of suspensions of ZnO nanoparticles (ZnO nanofluids). *Journal of Nanoparticle Research*, *9*(3), 479–489.
Zhang, Y., Chen, Y., Westerhoff, P., & Crittenden, J. (2009). Impact of natural organic matter and divalent cations on the stability of aqueous nanoparticles. *Water Research*, *43*(17), 4249–4257.